JOURNAL OF THEORETICAL AND APPLIED MECHANICS
48, 2, pp. 465-478, Warsaw 2010

ANALYSIS OF DAMPING OF VIBRATIONS THROUGH A FRICTIONAL DAMPER

Zbigniew Skup

Warsaw University of Technology, Institute of Machine Design Fundamentals, Warsaw, Poland
e-mail: zskup@ipbm.simr.pw.edu.pl

This paper presents a study of damping of non-linear vibrations in a one-degree-of freedom model of a mechanical system containing a friction damper. The vibrations of the system due to harmonic excitation is considered on the assumption of uniformly varying frequency and a constant amplitude of the exciting force. The simultaneous phenomenon of structural friction (passive damping) has been considered as well. The problem is considered on the assumption of a uniform unit pressure distribution between contacting surfaces of the friction conic inner and outer rings. The aim of the analysis is to asses the influence of angular acceleration, amplitude of the exciting force and the reduced mass on resonance curves during the start-off. The equations of motion of the examined system were solved by means of the Krylov-Bogolubov-Mitropolski method and digital simulation.

Key words: friction damper, structural friction, non-linear vibrations, resonance curves, starting-off vibrations

1. Introduction

The starting-off and braking phases are important moments in operation of every machine. During these processes, transition through the dangerous resonance zone can occur. The fundamental criterion in the design of friction dampers (Figs. 1, 2) or their combinations, such as frictional-elastomer ones, is to make them suitable for mechanical systems operating in dynamic conditions. Therefore, the appropriate selection of geometric parameters and loadings can serve as protection against going into dangerous resonances or it can considerably reduce the resonance amplitude by making use of the natural capacity of vibration damping in a given material. To determine such dependencies, a mathematical model has to be created to approximate the

real system. Traditional professional literature treats frictional torsion dampers, frictional clutches and brakes as joints of rigid bodies. The microsliding effect in the elastic range of the material of cooperating elements is called the structural friction. This phenomenon is well known and referred to as the structural hysteresis loop, see Gałkowski (1999), Giergiel (1990), Kaczmarek (2003), Kosior (2005), Mostowicz-Szulewski and Nizioł (1992), Osiński (1998), Sanitruk *et al.* (1997), Sextro (2002), Wang and Chen (1993). More advanced models are developed based mainly on finite elements, see Grudziński and Kostek (2005), Ostachowicz (1989), Zboiński and Ostachowicz (2001).

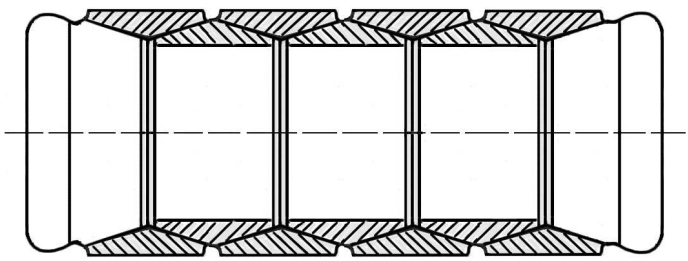

Fig. 1. Simplified model of a friction damper

The model of the friction damper adopted for analytical consideration (Fig. 1) is composed of cooperating conical surfaces of friction pairs consisting of inner and outer rings (Fig. 2). This type of friction dampers has been applied in ring buffers and friction dampers used to dissipate energy. Contact deformation, friction and damping of vibrations occurring in temporary fastenings and permanent joints have essential influence on dynamical properties of machines and devices. Mathematical description of the phenomenon of structural friction is not easy due to the complexity of the friction process and difficulties in describing the state of stresses and deformations occurring in the joints of elements. Therefore, the description is based on simplified assumptions and fundamental mechanical laws that apply to the patterns of stress and deformations arising in the process of bending, tension, compression, torsion, and shearing, see Gałkowski (1999), Giergiel (1990), Grudziński and Kostek (2005), Kosior (2005), Osiński (1998), Skup (1998), Zboiński and Ostachowicz (2001).

The following assumptions were made in order to analyse the friction damper: the distribution of unit pressure between cooperating surfaces in the rings contact joint is uniform and the friction coefficient of the contacting elements is constant for any value of unit pressure. Friction forces on the contact surfaces of cooperating elements are subject to the Coulomb law, and, consequently, the frictional resistance is proportional to pressure. The material properties are described by Hooke's law; the friction (kinetic or static) that occurs is

identical in the whole zone and depends on the state of load. Furthemore, flat sections were assumed (cross-sections remain flat after deformation of the elements). Apart from theoretical examination of the model shown in Fig. 2, experimental tests were conducted on the real system (Fig. 1).

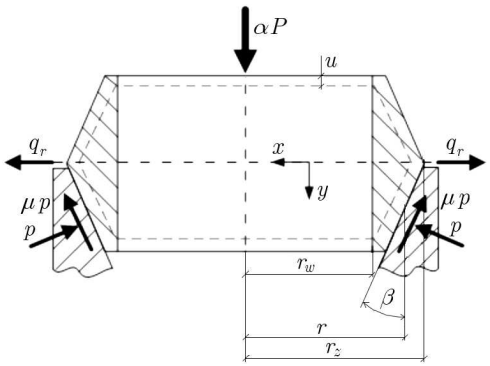

Fig. 2. Simplified model of the contact joint of the friction pair in a friction damper

The denotations used in Fig. 2 are: r – average radius of the conical surface of the rings, r_z, r_w – external and internal radii of the conical surface of the ring, β – angle of tilt of the conical surface, u – displacement, α – non-dimensional parameter ranging from 0 to 1, P – axial load, p – unit pressure per unit length, μ – friction coefficient.

Laboratory experiments on the test stand have shown that the rotational speed can be described quite precisely by the relation: $n(t) = \gamma t^2$ (parameter determined experimentally). Since the rotational speed is the square function of time, the amplitude of the resisting force is constant. It is assumed that the friction damper has been burdened with a load of constant value P_s as well as a variable component $P(t)$ in form of harmonic excitation by a force having a constant amplitude P_0 with uniformly varying angular velocity of the excitation $\omega(t)$. Therefore, the overall load P_c takes the following form

$$\begin{aligned} P_c &= P_s + P(t) & P(t) &= P_0 \sin\theta \\ \theta &= \frac{\varepsilon t^2}{2} + \xi & \omega(t) &= \frac{d\theta}{dt} = \varepsilon t \end{aligned} \tag{1.1}$$

where θ is the phase angle of excitation, ε – angular acceleration at the start-off, ξ – phase shift angle, t – time.

The application of the Krylov-Bogolubov-Mitropolski asymptotic method, as presented, for instance, in Mitropolskij (1964), Osiński (1979, 1998) and Skup (1998) made it possible to eliminate the function $\operatorname{sgn}\dot{u}$, which is troublesome in numerical simulations.

2. Equation of motion of the examined system

The model adopted for analytical considerations is a one-degree-of-freedom mechanical system with a nonlinear hysteresis loop of a duplex triangle shape, see the friction damper shown in Fig. 1.

The differential equation of motion of the examined system can be written as follows

$$m\ddot{u} + P(u, \operatorname{sgn}\dot{u}) = P_c \tag{2.1}$$

where m is the reduced mass of the examined system, u – coordinate of displacement of the reduced mass, $P(u, \operatorname{sgn}\dot{u})$ – force in a cycle represented by the structural hysteresis loop (Fig. 3) dependent on the relative displacement u, amplitude and sign of the velocity $\dot{u}$.

In order to apply the asymptotic Krylov-Bogolubov-Mitropolski method, it is necessary to transform the function $P(u, \operatorname{sgn}\dot{u})$. Thus, after some manipulations, the function $P(u, \operatorname{sgn}\dot{u})$ takes the form

$$P(u, \operatorname{sgn}\dot{u}) = ku - \nu F\Big(u, \frac{du}{dt}\Big) \tag{2.2}$$

Therefore, differential equation of motion (2.1) assumes a form

$$m\ddot{u} + ku = \nu F\Big(u, \frac{du}{dt}\Big) + P_c \tag{2.3}$$

where $k = P_0/u$ is the stiffness of compression, ν – small non-dimensional parameter.

The solution to non-linear differential equation (2.3), which describes motion of the examined system, is assumed in the first approximation as

$$u = A\cos(\theta + \xi) \tag{2.4}$$

By incorporating the asymptotic method (see Mitropolski, 1964; Osiński, 1979), we can obtain a system of differential equations describing the amplitude of the angular displacement A and the phase shift ξ as given below

$$\frac{dA}{dt} = \nu A_1(t, A, \xi) \qquad \frac{d\xi}{dt} = \omega_0 - \omega(t) + \nu B_1(t, A, \xi) \tag{2.5}$$

Therefore, the natural frequency ω_0 of the system can described by the formula

$$\omega_0 = \sqrt{\frac{k}{m}} \tag{2.6}$$

The first and second derivative of (2.4) takes the form

$$\begin{aligned}
&\frac{du}{dt} = \nu A_1 \cos(\theta+\xi) - \omega_0 \sin(\theta+\xi) - A\nu B_1 \sin(\theta+\xi)\\
&\frac{d^2u}{dt^2} = \nu\Big[(\omega_0-\omega)\frac{\partial A_1}{\partial \xi} - 2A\omega_0 B_1\Big]\cos(\theta+\xi) - A\omega_0^2\cos(\theta+\xi) +\\
&\quad -\nu\Big[(\omega_0-\omega)A\frac{\partial B_1}{\partial \xi} + 2A_1\omega_0\Big]\sin(\theta+\xi) +\\
&\quad +\nu^2\cos(\theta+\xi)\Big[A_1\frac{\partial A_1}{\partial A} + B_1\frac{\partial A_1}{\partial \xi} - AB_1^2\Big] +\\
&\quad -\nu^2\sin(\theta+\xi)\Big[2A_1B_1 + AA_1\frac{\partial B_1}{\partial A} + AB_1\frac{\partial B_1}{\partial \xi}\Big] +\\
&\quad +\nu\Big[\frac{\partial A_1}{\partial t}\cos(\theta+\xi) - A\frac{\partial B_1}{\partial t}\sin(\theta+\xi)\Big]
\end{aligned} \tag{2.7}$$

The displacements and deformations of the examined model are small and therefore the solution to differential equation (2.3) is adopted for considerations as the first approximation. Taking that into account, the expressions in which the parameter ν appears in the second or a higher power can be neglected. It is necessary to add that, due to the state of equilibrium of the considered system, the expressions at the secular terms $\cos(\theta+\xi)$ and $\sin(\theta+\xi)$ should amount to zero (the mechanical system is stable then). In this case, the value of the parameter ν is very small, thus it is neglected in final considerations.

Finally, equation $(2.7)_2$ takes the following form

$$\begin{aligned}
&\frac{d^2u}{dt^2} = \nu\Big[(\omega_0-\omega)\frac{\partial A_1}{\partial \xi} - 2A\omega_0 B_1\Big]\cos(\theta+\xi) - A\omega_0^2\cos(\theta+\xi) +\\
&\quad -\nu\Big[(\omega_0-\omega)A\frac{\partial B_1}{\partial \xi} + 2A_1\omega_0\Big]\sin(\theta+\xi)
\end{aligned} \tag{2.8}$$

Substituting formulas (2.4) and (2.8) to the left-hand side of equation (2.3), we obtain

$$\begin{aligned}
&\Big\{m\frac{d^2u}{dt^2} + ku\Big\}_{u=A\cos(\theta+\xi)} = m\nu\Big[(\omega_0-\omega)\frac{\partial A_1}{\partial \xi} - 2A\omega_0 B_1\Big]\cos(\theta+\xi) +\\
&\quad -m\nu\Big[(\omega_0-\omega)A\frac{\partial B_1}{\partial \xi} + 2A_1\omega_0\Big]\sin(\theta+\xi)
\end{aligned} \tag{2.9}$$

After averaging during one period of time of the main harmonic angle $(\theta+\xi)$, the right-hand side of equation (2.3) can be presented as follows

$$\begin{aligned}
&\Big\{\nu F\Big(u,\frac{du}{dt}\Big)+P_0\sin\theta+P_s\Big\}_{u=A\cos(\theta+\xi)}=\\
&\quad=\frac{\nu\cos(\theta+\xi)}{\pi}\int_0^{2\pi}F(A\cos(\theta+\xi),-A\omega_0\sin(\theta+\xi))\cos(\theta+\xi)\;d(\theta+\xi)+\\
&\quad+\frac{\nu\sin(\theta+\xi)}{\pi}\int_0^{2\pi}F(A\cos(\theta+\xi),-A\omega_0\sin(\theta+\xi))\sin(\theta+\xi)\;d(\theta+\xi)+\\
&\quad+P_0(\cos\xi\sin(\theta+\xi)-\sin\xi\cos(\theta+\xi))
\end{aligned}\tag{2.10}$$

Having compared the coefficients at identical powers ν and, relevantly, at sines and cosines of the right-hand sides of equations (2.9) and (2.10), after some transformations of the expressions for $A_1(t,A,\xi)$ and $B_1(t,A,\xi)$, we obtain a system of equations from which the functions A_1 and B_1 can be determined

$$\begin{aligned}
A_1(t,A,\xi)&=-\frac{1}{2\pi m\omega_0}\int_0^{2\pi}F_0(A,\chi)\sin\chi\;d\chi-\frac{P_0\cos\xi}{\nu m[\omega_0+\omega(t)]}\\
B_1(t,A,\xi)&=-\frac{1}{2\pi m\omega_0 A}\int_0^{2\pi}F_0(A,\chi)\cos\chi\;d\chi+\frac{P_0\sin\xi}{\nu mA[\omega_0+\omega(t)]}
\end{aligned}\tag{2.11}$$

where

$$F_0(A,\chi)=P(u,\dot u)=F(A\cos\chi,-A\omega_0\sin\chi)\qquad\qquad\chi=\theta+\xi\tag{2.12}$$

Substituting formulae (2.11) into the system of equations (2.5) and rearranging them, we obtain

$$\begin{aligned}
\frac{dA}{dt}&=-\frac{\nu}{2\pi m\omega_0}\int_0^{2\pi}F_0(A,\chi)\sin\chi\;d\chi-\frac{P_0}{m(\omega_0+\omega)}\cos\xi\\
\frac{d\xi}{dt}&=\omega_0-\omega(t)-\frac{\nu}{2\pi m\omega_0 A}\int_0^{2\pi}F_0(A,\chi)\cos\chi\;d\chi+\frac{P_0}{mA(\omega_0+\omega)}\sin\xi
\end{aligned}\tag{2.13}$$

As in works by Mitropolski (1964) – formula 3.53, p. 91 and Osiński (1979) – formulae 2.150, 2.151, p. 65, the equivalent frequency $\omega_{0eq}(A)$ and equivalent

damping coefficient of vibrations $h_{eq}(A)$ were introduced into the system of equations (2.13). Thus, this system takes the form

$$\begin{aligned} \frac{dA}{dt} &= -h_{eq}(A)A - \frac{P_0}{m(\omega_0+\omega)}\cos\xi \\ \frac{d\xi}{dt} &= \omega_{0eq}(A) - \omega(t) + \frac{P_0}{mA(\omega_0+\omega)}\sin\xi \end{aligned} \tag{2.14}$$

where

$$\begin{aligned} h_{eq}(A) &= \frac{\nu}{2\pi m\omega_0}\int_0^{2\pi} F_0(A,\chi)\sin\chi\, d\chi \\ \omega_{0eq}(A) &= \omega_0 - \frac{\nu}{2\pi m\omega_0 A}\int_0^{2\pi} F_0(A,\chi)\cos\chi\, d\chi \end{aligned} \tag{2.15}$$

Because of the discontinuity of the function $P(u, \operatorname{sgn}\dot{u})$ at $\dot{u}=0$, we confine the analysis to one half-period of the vibrating motion (the motion between four stops). Thus, the integration interval $(0, 2\pi)$ will be divided into four sub-intervals.

The influence of the elasticity and frictional parameters k_1 and k_2, which equal $\tan\xi_1$ and $\tan\xi_2$ respectively, on the damping properties of the investigated system is shown in Fig. 3.

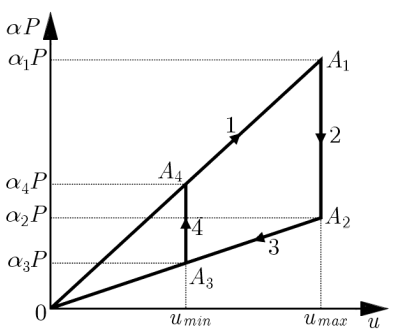

Fig. 3. Hysteretic loop for the friction pair of the ring spring

The tests were conducted on the MTS testing machine at the Institute of Machine Design Fundamentals at Warsaw University of Technology with the use of the Test Ware SX software. The methodology of the experiment consisted in loading the system up to the maximum value P_{max} so that not

to exceed the safe limit of the material elasticity. Next, the system was unloaded down to the pre-assumed value P_{min} and re-loaded again (Fig. 4). Before the measurement began, both the extensometer and the control-measurement system were subject to calibration. The method and the results of the investigations are described in (Skup, 2007)

$$k_1 = \tan\xi_1 = \frac{P_1}{u_{max}} \qquad k_2 = \tan\xi_2 = \frac{P_2}{u_{max}} \tag{2.16}$$

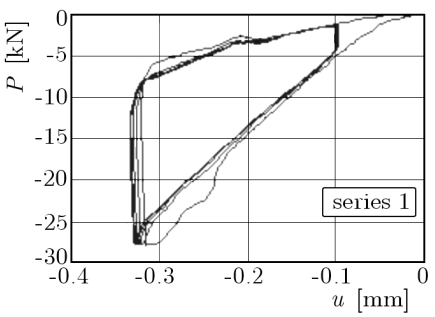

Fig. 4. Experimental hysteretic loop: loading force $P_{max} = 28\,\text{kN}$, number of loading and unloading cycles 4

Based on the graph in Fig. 3, $P_1 = P$ for $\alpha = 1$, whereas $P_2 = \alpha_2 P$, the maximum displacement u_{max} for the final stage of the load $\alpha = 1$ (see line OA_1 in Fig. 3) and non-dimensional parameter α_2 can be determined on the basis of the formulae derived by the author (Skup, 2007 – formulae 2.7, p. 365, and 2.11, p. 367), therefore

$$u_{max} = \frac{2Pr}{\pi EF}\left(\frac{c\tan\beta - \mu}{\tan\beta + \mu}\right) \qquad \alpha_2 = \frac{(\cot\beta - \mu)(\tan\beta - \mu)}{(\tan\beta + \mu)(\cot\beta + \mu)} \tag{2.17}$$

where E is Young's modulus, F – area of cross-section of the rings.

- 1st stage of motion from 0 to $\pi/2$, $P(u, \operatorname{sgn}\dot{u}) = k_2 u$, $\dot{u} < 0$, $u > 0$
- 2nd stage of motion from $\pi/2$ to π, $P(u, \operatorname{sgn}\dot{u}) = k_1 u$, $\dot{u} < 0$, $u < 0$
- 3rd stage of motion from π to $3\pi/2$, $P(u, \operatorname{sgn}\dot{u}) = k_2 u$, $\dot{u} > 0$, $u < 0$
- 4th stage of motion from $3\pi/2$ to 2π, $P(u, \operatorname{sgn}\dot{u}) = k_1 u$, $\dot{u} > 0$, $u > 0$

After finding the integrals in system of equations (2.13) and having used above conditions, we obtain

$$\begin{aligned}
&\int_0^{2\pi} F_0(A,\chi)\sin\chi\,d\chi = \int_0^{\pi/2} k_2 u\sin\chi\,d\chi + \int_{\pi/2}^{\pi} k_1 u\sin\chi\,d\chi + \\
&\quad + \int_{\pi}^{3\pi/2} k_2 u\sin\chi\,d\chi + \int_{3\pi/2}^{2\pi} k_1 u\sin\chi\,d\chi = A(k_2-k_1) \\
&\int_0^{2\pi} F_0(A,\chi)\cos\chi\,d\chi = \int_0^{\pi/2} k_2 u\cos\chi\,d\chi + \int_{\pi/2}^{\pi} k_1 u\cos\chi\,d\chi + \\
&\quad + \int_{\pi}^{3\pi/2} k_2 u\cos\chi\,d\chi + \int_{3\pi/2}^{2\pi} k_1 u\cos\chi\,d\chi = \frac{\pi A(k_1+k_2)}{2}
\end{aligned} \tag{2.18}$$

Substituting (26) into $(2.15)_1$ and (27) into $(2.15)_2$, we obtain

$$h_{eq}(A) = \frac{\nu A(k_2-k_1)}{2\pi m\omega_0} \qquad \omega_{0eq}(A) = \omega_0 - \frac{\nu\pi A(k_1+k_2)}{4\pi m\omega_0 A} \tag{2.19}$$

Finally, the system of differential equations (2.14), if we make use of (2.19), takes the following form

$$\begin{aligned}
\frac{dA}{dt} &= \frac{\nu A}{2\pi m\omega_0}(k_1-k_2) - \frac{P_0\cos\xi}{m(\omega_0+\omega)} \\
\frac{d\xi}{dt} &= \omega_0 - \omega - \frac{\nu(k_1+k_2)}{4m\omega_0} + \frac{P_0\sin\xi}{mA(\omega_0+\omega)}
\end{aligned} \tag{2.20}$$

Finally, in two basic differential equations (2.20) we have an expression for the relative displacement amplitude A (vibration amplitude) as function of the excitation frequency ω (the resonance curves for initial vibrations). The influence of the angular acceleration, the exciting force amplitude and reduced mass on the resonance curves during the start-off of the system has been investigated.

3. Numerical investigations

Differential system of equations (2.20) has been solved by means of the Runge-Kutta method of the fourth order with Gill's modification (the program library of PDP RT 11 company, Subroutine RKGS). In order to compare the numerical

results, the Mathematica 4.1 software has been used to work out a comparing program in Borland C++ environment.

The results obtained from computer simulations concerning the non-stationary (transient) state of forced vibrations in the friction damper are shown in Figs. 5, 6, 7. Numerical calculations carried out for the above formulae incorporated the basic geometrical parameters and material properties of the examined friction damper given in Table 1.

Table 1. Data for numerical calculations

No.	Parameter [unit]	Value
1	Loading force $P_1 = P$ [N]	28000
2	Non-dimensional parameter α_1	1
3	Non-dimensional parameter α_2 for $\beta = 12°$	0.0280476
4	Non-dimensional parameter α_2 for $\beta = 14°$	0.0993034
5	Non-dimensional parameter α_2 for $\beta = 16°$	0.1588123
6	Non-dimensional parameter α_2 for $\beta = 18°$	0.208914
7	Young's modulus E [N/mm^2]	$2.1 \cdot 10^5$
8	Friction coefficient μ	0.20
9	Angle of tilt of cones β [°]	12, 14, 16, 18
10	External radius of ring r_z [mm]	38.5
11	Internal radius of ring r_w [mm]	31.5
12	Average radius of conical surface of ring r [mm]	37.25
13	Cross-sectional area of rings F [mm^2]	132.94
14	Reduced mass m [kg]	0.443

The basic values of quantities describing the initial, non-stationary state of the system are included in Table 2.

Table 2. Results of numerical calculations

Angle β [°]	Force P_1 [N]	Force P_2 [N]	Displacement u_{max} [mm]
12	28000	785.33	0.260
14	28000	2780.50	0.202
16	28000	4446.74	0.161
18	28000	5849.59	0.130

In technical cases of starting-off or braking conditions mechanical systems, the frequency of the force which excites system vibration permanently changes. Transition through the resonance zone may appear in such circumstances

(Fig. 5-7). During the initial stage, resonance curves in the pre-resonance (sub-resonant) and, especially, post-resonance (super-resonant) period may differ considerably. The resonance curves show that during the starting-off stage of the mechanical system, the post-resonance amplitudes are lower than the pre-resonance ones and they have an oscillating character. The graphs indicate that when the value of angular acceleration ε and the amplitude of excitation force P_0 increase, the resonance amplitudes move towards greater values of the excitation frequencies. In Fig. 5, we can see a relation of the vibration amplitude A versus excitation frequency ω for different angular accelerations. The resonant amplitudes decrease with the increase of the angular acceleration ε. We can also observe the beating phenomenon before and after the resonance. Shifting of the resonances towards higher frequencies is brought about by the retardation effect (as mentioned in the previous section). The observed shift for increasing values of ε results from the retardation effect of the region of maximum amplitudes with respect to the natural frequency (see Fig. 5). It is the known effect of transitory resonance, also observed in linear systems.

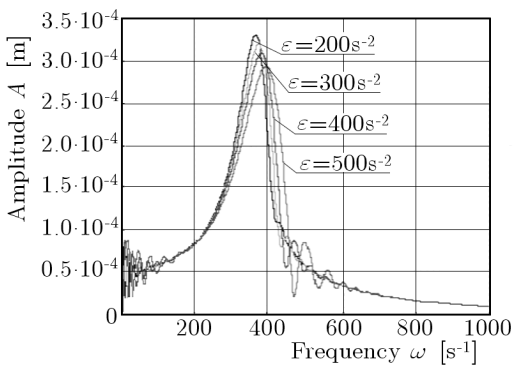

Fig. 5. Graphs of resonant curves for different values of the angular acceleration ε

The analysis of graphs presented in Fig. 6 indicates that greater values of P_0 imply higher levels of vibration amplitudes and a slight shift of the resonant frequencies toward smaller frequencies. In the case of a deterministic excitation, the existence of resonance curves corresponding to decaying super-resonant vibration confirms the peculiarity of the resonant transition.

The influence of the reduced mass m on the resonance vibration amplitude A in function of the excitation frequency ω is essential and is shown in Fig. 7. The increasing value of the reduced mass leads to a smaller value of the main vibration resonance amplitude as well as dislocation of the amplitude towards smaller values of the excitation frequency (Fig. 7).

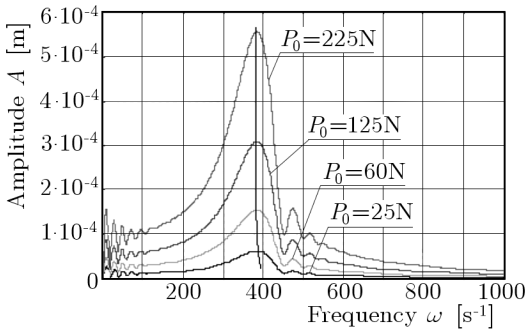

Fig. 6. Graphs of resonant curves for different excitation amplitudes P_0

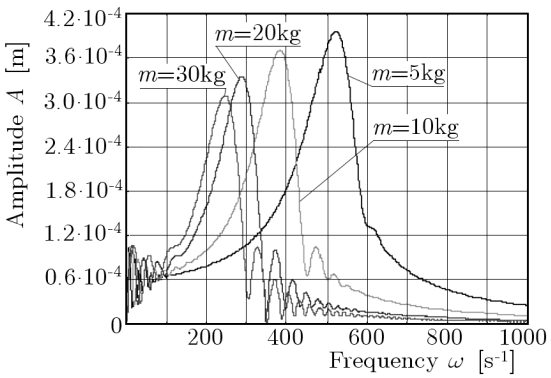

Fig. 7. Graphs of resonant curves for different values of the reduced mass m

4. Concluding remarks

Structural friction between the contacting surfaces of internal and external rings of the examined damper increases the damping of vibrations in the examined system. The damping effect is the greatest for an appropriate value of the friction force because the zone of the relative slip between the internal and external rings of the friction damper is the largest. The efficiency of vibration damping by means of the friction damper is greatly influenced by the following factors: exciting force, friction force (unit pressure, friction coefficient), angular acceleration, stiffness of the internal and external rings, reduced mass. The effects of structural friction can be employed to enrich the design methods of dynamical systems.

On the basis of the obtained results, it has been found that all resonance curves always start from a non-zero resonance amplitude and tend asympto-

tically to zero in the post-resonance range. The simulations also confirmed a certain peculiarity when the system passes through the resonance. The peculiarity, indicated in works by Mitropolskij (1964), Osiński (1998) and Skup (1998), has form of a decaying "beating" phenomenon. It vanishes after some time, and the amplitude rests on a level that is usually smaller than that in the sub-resonant zone.

References

1. Gałkowski Z., 1999, Wpływ tarcia konstrukcyjnego na drgania wału z tuleją, *Zesz. Nauk. Politechniki Rzeszowskiej*, **174**, 283-288
2. Giergiel J., 1990, *Tłumienie drgań mechanicznych*, PWN, Warszawa
3. Grudziński K., Kostek R., 2005, Influence of normal micro-vibrations in contact on sliding motion of solid body, *Journal of Theoretical and Applied Mechanics*, **43**, 37-49
4. Kaczmarek W., 2003, Analysis of a bolted joint with elastic and frictional effects occurring between its elements, *Machine Dynamics Problems*, **27**, 1, 157-167
5. Kosior A., 2005, Wpływ parametrów wybranych połączeń z tarciem konstrukcyjnym na właściwości sprężysto-tłumiące układów mechanicznych, *Prace Naukowe, Mechanika*, **209**, Oficyna Wydawnicza Politechniki Warszawskiej, Warszawa
6. Mitropolskij Ju.A., 1964, *Problemy asimptoticheskoj teorii nestacjonarnykh kolebanii*, Izdat. Nauka, Moskwa
7. Mostowicz-Szulewski J., Nizioł J., 1992, Forced steady-state and nonstationary vibrations of a beam with bilinear hysteresis and hysteresis in fixing, *Nonlinear Vibration Problems*, **24**, 33-62
8. Osiński Z., 1979, *Teoria drgań*, PWN, Warszawa
9. Osiński Z., 1998, *Damping of Vibrations*, A.A. Balkema, Rotterdam/Brookfield
10. Ostachowicz W., 1989, Forced vibrations of a beams including dry friction dampers, *An Int. J. Computers and Structures*, **22**, 851-858
11. Sanitruk K.Y., Imregun M., Ewins D.J., 1997, Harmonic balance vibration analysis of turbine blades with friction dampers, *Journal of Vibration and Acoustics*, **119**, 96-103
12. Sextro W., 2002, *Dynamical Contact Problems with Friction*, Springer, Berlin

13. Skup Z., 1998, Wpływ tarcia konstrukcyjnego w wielotarczowym sprzęgle ciernym na drgania w układzie napędowym, *Prace naukowe, Mechanika*, **167**, Oficyna Wydawnicza PW (Ph. Dsc. disertation)

14. Skup Z., 2007, Theoretical and experimental studies of energy dissipation in a model of a ring spring, Journal of Theoretical and Applied Mechanics, **45**, 2, 363-377

15. Wang J.H., Chen W.K., 1993, Investigation of the vibration of a blade with friction damper by HBM, *J. of Engineering for Gas Turbines and Power*, **115**, 294-299

16. Zboiński G., Ostachowicz W., 2001, Three-dimensional elastic and elastoplastic frictional contact analysis of turbomachinery blade attachments, *J. of Theoretical Applied Mechanics*, **39**, 769-790

Analiza tłumienia drgań poprzez tłumik cierny

Streszczenie

W pracy przedstawiono badania tłumienia drgań nieliniowych układu mechanicznego o jednym stopniu swobody zawierającego amortyzator cierny. Rozważany jest rozruch układu przy wymuszeniu harmonicznym z jednostajnie zmienną częstością o stałej amplitudzie siły wymuszającej. Uwzględniono tłumienie drgań, wykorzystując zjawisko tarcia konstrukcyjnego (tłumienie pasywne). Zagadnienie rozpatrywane jest przy założeniu równomiernego rozkładu nacisków jednostkowych występujących pomiędzy współpracującymi stożkowymi powierzchniami ciernymi pierścieni tłumika. Zbadano wpływ przyspieszenia kątowego, amplitudy siły wymuszającej drgania oraz masy zredukowanej na krzywe rezonansowe drgań rozruchowych. Równania ruchu badanego układu mechanicznego rozwiązano wykorzystując asymptotyczną metodę Kryłowa-Bogolubowa-Mitropolskiego i metodę symulacji cyfrowej.

Manuscript received July 3, 2009; accepted for print October 27, 2009